International Journal of Thermal Sciences 48 (2009) 1718–1727

Contents lists available at ScienceDirect

International Journal of Thermal Sciences

journal homepage: www.elsevier.com/locate/ijts

Analysis of transient heat transfer in multilayer thin films with nonlinear thermal boundary resistance

K. Ramadan [a,*], M.A. Al-Nimr [b]

[a] Department of Mechanical Engineering, Mu'tah University, P.O. Box 7, Karak 61710, Jordan
[b] Department of Mechanical Engineering, Jordan University of Science and Technology, P.O. Box 3030, Irbid 22110, Jordan

ARTICLE INFO

Article history:
Received 6 March 2008
Received in revised form
26 November 2008
Accepted 26 January 2009
Available online 16 March 2009

Keywords:
Dual-phase-lag
Non-linear thermal boundary resistance
Heat conduction
Thin films
Thermal wave

ABSTRACT

Transient energy transport in thin-layer films with a nonlinear thermal boundary resistance is analyzed theoretically within the framework of the dual-phase-lag heat conduction model. An iterative finite difference numerical method is used and is verified using a derived semi-analytical solution of the problem. Effects of the thermo-physical properties on energy transport when a two-layer film is exposed to a thermal pulse of certain duration and strength are presented. The thermal boundary resistance, the heat flux and temperature gradient phase lags and the thermal conductivities and heat capacities all are important factors that characterize energy transport through the interface and the temperature distribution in the two layers. The maximum interfacial temperature difference that takes place in the transient process of thermal pulse propagation is found to be the proper choice to measure the perfect-ness of the interface with a finite thermal boundary resistance. The results show that even with high values of the thermal boundary resistance the maximum interfacial temperature difference can be very small when the thermal pulse propagates from a high-thermal conductivity and heat capacity layer to a low-thermal conductivity and heat capacity layer. For a certain range of the thermal conductivities and heat capacities, the maximum interfacial temperature difference approaches zero even with high values of the thermal boundary resistance. Thermal conductivities and heat capacities are much more important in characterizing transient heat transfer through the imperfect interface than the phase lags of the heat flux and temperature gradient.

1. Introduction

The thermal resistance existing at the interface between two materials has a significant effect on the design and performance of devices using multilayer thin films such as superconductors and microelectronic layer packages, where heat dissipation is a crucial issue that limits the performance, reliability and further miniaturization of these devices [1]. Thermal interface materials (TIM) that reduce or eliminate the micro-gaps at the interface between material layers [1,2] are used to reduce the thermal resistance in order to have more efficient heat management in such devices. The existence of a thermal resistance at the interface between adjacent layers results in a temperature difference the magnitude of which is in fact a measure of the temperature gradient at the interface. High temperature gradients can cause a thermal damage if the difference in temperature at the interface is not kept to a minimum. Hence, the choice of the materials with the proper thermal properties that result in a minimum interfacial temperature difference (and hence minimum interfacial temperature gradient) becomes crucial in the design of thin film structures particularly when the designer does not have much control over the reduction of the thermal boundary resistance.

Prediction of the thermal boundary resistance both theoretically and experimentally has received much attention [3–6] with the advancements of miniaturization technology. The diffuse mismatch model (DMM) which assumes that all phonons incident on the interface will scatter, and the acoustic mismatch model (AMM) which assumes no phonon scattering [3,7] are both used to predict the thermal boundary resistance at the interface between films where in both models the thermal resistance varies inversely with the third power of the temperature [3,8].

The amount of heat flowing through the interface between two material layers as well as the temperature gradient at the interface are however functions of not only the thermal boundary resistance but also of the thermo-physical properties of the materials. The use of suitable materials with certain thermo-physical properties can

* Corresponding author. Tel.: +962 3 2372380.
E-mail addresses: rkhalid@mutah.edu.jo (K. Ramadan), malnimr@just.edu.jo (M.A. Al-Nimr).

1290-0729/$ – see front matter © 2009 Elsevier Masson SAS. All rights reserved.
doi:10.1016/j.ijthermalsci.2009.01.014

Nomenclature

c_j	heat capacity of layer j, J/m^3 K
f	time dependent boundary heat flux, W/m^2
F	dimensionless time dependent boundary heat flux
$\overline{F}$	Laplace transform of F
k_j	dimensionless thermal conductivity ratio of layer j, $\tilde{k}_j/k_r$
L	domain width, m
ℓ_j	dimensionless width of layer j, $L/\sqrt{\alpha_r\tilde{\tau}_{qr}}$
p	Laplace transform parameter
$\overrightarrow{q}$	heat flux vector, W/m^2
q	heat flux, W/m^2
Q	dimensionless heat flux, $q/[c_rT_r\sqrt{\alpha_r/\tilde{\tau}_{qr}}]$
$\overline{Q}$	Laplace transform of Q
$\overrightarrow{r}$	position vector
R_b	dimensionless thermal boundary resistance
T	temperature, K
T_j^o	initial temperature of layer j, K
x	x-coordinate

Greek letters

α_j	thermal diffusivity of layer j, m^2/s
α_j	dimensionless thermal diffusivity, α_j/α_r
$\Delta\theta_I$	temperature difference at the contact interface
$\Delta\theta_{I,\max}$	maximum interfacial temperature difference
ε	convergence criterion
ζ	dimensionless distance, $x/\sqrt{\alpha_r\tilde{\tau}_{qr}}$
ℓ_j	dimensionless width of layer j, $L/\sqrt{\alpha_r\tilde{\tau}_{qr}}$
η	dimensionless time, $t/\tilde{\tau}_{qr}$
θ	dimensionless temperature, $(T-T_r)/T_r$
θ_j^o	dimensionless initial temperature of layer j
$\overline{\theta}$	Laplace transform of θ
$\tilde{\tau}_{qj}$	heat flux phase lag of layer j, s
τ_{qj}	dimensionless heat flux phase lag of layer j, $\tilde{\tau}_{qj}/\tilde{\tau}_{qr}$
$\tilde{\tau}_{Tj}$	temperature gradient phase lag of layer j, s
τ_{Tj}	dimensionless temperature gradient phase lags for layer j, $\tilde{\tau}_{Tj}/\tilde{\tau}_{qr}$
κ	a constant parameter, W/m^2 K^4

Subscripts

j	layer (or domain) j
r	reference value

Superscripts

p	previous iteration
n	Previous time level
$n+1$	Current time level

have a significant role in determining the amount of heat flow and temperature gradient at the interface between layers in contact with a thermal boundary resistance.

Applications where extremely short times, high power intensity or cryogenic temperatures are experienced mandates modeling transient heat transfer on a micro-scale level in space and time, since the parabolic heat diffusion model is known to break down in such applications. The dual-phase-lag (DPL) heat conduction model developed and experimentally supported by Tzou [9,10] accounts for spatial and temporal effects in both macro- and micro-scale heat transfer in a one-temperature formulation and it takes the form:

$$\overrightarrow{q}\left(\overrightarrow{r},t+\tilde{\tau}_q\right) = -\tilde{k}\nabla T\left(\overrightarrow{r},t+\tilde{\tau}_T\right)$$

The quantities $\tilde{\tau}_q$ and $\tilde{\tau}_T$ in this model are respectively, the phase lags of the heat flux and the temperature gradient. The DPL model reduces to the classical Fourier's heat diffusion model, thermal wave model, phonon–electron interaction, and phonon scattering models by assigning the proper values to the phase lags $\tilde{\tau}_q$ and $\tilde{\tau}_T$. The DPL model therefore covers a wide range of transient thermal responses from macroscopic to microscopic scales in both time and space. The classical parabolic Fourier's heat diffusion is recovered from the DPL when the two phase- lags $\tilde{\tau}_q$ and $\tilde{\tau}_T$ are equal, where the heat flux and the temperature gradient occur simultaneously. The thermal wave model that describes the wave nature of energy transport is also a special case of the DPL model by setting $\tilde{\tau}_T = 0$ with $\tilde{\tau}_q > 0$. The phonon–electron interaction model that results in enhanced or over-diffusion nature of energy transport is obtained with non-zero values of both $\tilde{\tau}_q$ and $\tilde{\tau}_T$ with $\tilde{\tau}_q < \tilde{\tau}_T$ [9]. The DPL model also reduces to the phonon-scattering model by relating $\tilde{\tau}_q$ and $\tilde{\tau}_T$ in the dual-phase-lag model to the relaxation times in the phonon-scattering model [9]. The energy equation within the framework of the DPL model with $\tilde{\tau}_q > \tilde{\tau}_T > 0$ describes the combined diffusion- and thermal wave- mechanisms of energy transport where the relative significance of the two mechanisms is controlled by the values of $\tilde{\tau}_q$ and $\tilde{\tau}_T$.

Transient heat transfer in multilayered materials with perfect (zero thermal boundary resistance) and imperfect interfaces has been studied using different micro-scale heat transfer models including the DPL model. Ho et al. [11] analyzed heat transfer with a pulsed volumetric heat source in multilayered structure in perfect thermal contact and showed the effect of the temperature gradient phase lag on energy transport through the perfect interface using the lattice Boltzmann numerical method. Al-Huniti and Al-Nimr [12] investigated the thermo-elastic behavior of a two-layered metallic thin plate in perfect thermal contact using the dual-phase-lag model. Lee and Tsai [13] used the DPL model to study the thermal behavior in a two-layered semi-infinite layers with interfacial contact conductance (the reciprocal of the thermal resistance) using a simple temperature jump condition at the interface. They examined the lagging behavior of a two-layer material, and the effect of the constant contact conductance and the thickness of the surface layer on heat transfer in the structure. The DPL model was also used to investigate the thermal behavior of two-layered planar thin slabs in perfect contact with a periodic heating source and a periodic boundary temperature [14]. Closed-form solutions were derived to study the deviations among the predictions of the classical heat diffusion, thermal wave and the DPL models. A study of thermal wave propagation in a composite sphere with perfect contact subject to a sudden temperature change on the outer surface was investigated by Tsai and Hung [15] using the hyperbolic heat conduction model. Lor and Chu [8] used the thermal wave model to study the effect of the interfacial thermal resistance on heat transfer in a composite medium using a radiation boundary condition at the interface. Liu [16] investigated the thermal behavior of layered films with a nonlinear interfacial thermal resistance using a hybrid application of the Laplace transform and control volume techniques. Heat transfer in his analysis was induced by a pulsed volumetric heat source adjacent to the exterior surface of one layer. His results show that the effect of the thermo-physical properties on energy transport through the interface gradually decreases with increasing the interfacial thermal

resistance. The hyperbolic two-step model was also used by Liu [17] to analyze the thermal behavior of multilayer metal thin films with a zero interfacial thermal boundary resistance. The thermal wave model was used by Khadrawi et al. [18] to study the thermal behavior of perfect and imperfect contact composite slabs with a constant interfacial thermal resistance.

The DPL model is used in this work to study transient heat transfer processes in two-layer thin films with nonlinear thermal boundary resistance. For a vanishing thermal boundary resistance, the interfacial temperature jump approaches zero and the interface behaves perfectly, while for an infinite value of the thermal boundary resistance, the interface experiences the highest temperature jump since the interface behaves as a perfect insulator. One choice to measure the relative perfect-ness of the interface with a finite nonlinear thermal boundary resistance is thus the interfacial temperature difference. The temperature jump and heat flux at the imperfect interface are dependent on the value of the thermal boundary resistance, the thermal conductivities and heat capacities of the two layers as well as the nature of energy transport represented by the phase lags of the heat flux and temperature gradient as discussed previously. The concentration in this work is particularly on the effects of the thermo-physical properties and the nature of energy transport on the interfacial temperature jump as well as temperature and heat flux distributions in two-layer thin films with a temperature dependent thermal boundary resistance when one layer is exposed to an external thermal pulse of short duration and finite strength.

2. Physical model and problem formulation

The problem geometry in this work is as shown in Fig. 1. The geometry is made up of a planar slab of two layers in contact with a thermal boundary resistance at the interface between the two layers. The left surface of layer 1 is assumed to have negligible heat loss (insulated), while the right surface of layer 2 is exposed to a time-dependent thermal pulse with a certain duration and strength. The energy equation for layer j of the two-layer slab shown in Fig. 1 is:

$$c_j\frac{\partial T_j}{\partial t}+\frac{\partial q_j}{\partial x}=0,\quad j=1,2 \tag{1}$$

where q_j is given by the dual-phase-lag heat conduction model [9]:

$$q_j+\tilde{\tau}_{qj}\frac{\partial q_j}{\partial t}=-\tilde{k}_j\left[\frac{\partial T_j}{\partial x}+\tilde{\tau}_{Tj}\frac{\partial^2 T_j}{\partial t\partial x}\right],\quad j=1,2 \tag{2}$$

and the boundary conditions are:

$$q_1(x,0)=0 \tag{3}$$

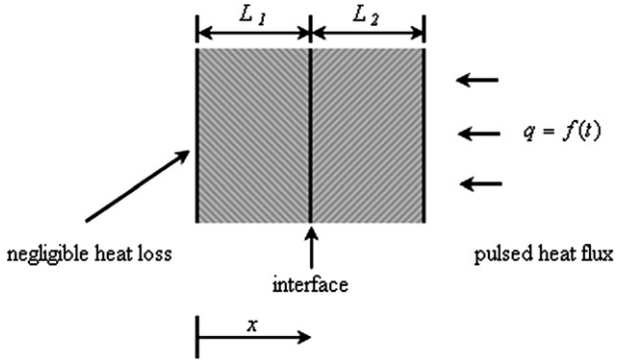

Fig. 1. Illustration of problem geometry and boundary conditions.

$$q_2(L_1+L_2,t)=f(t) \tag{4}$$

where $f(t)$ is a time-dependent boundary heat flux.

The two layers are assumed to be initially at uniform temperatures:

$$T_j(x,0)=T_j^o,\quad j=1,2 \tag{5}$$

At the interface between the two layers, the heat flux is continuous while the thermal boundary resistance causes an interfacial temperature difference that is dependent on the thermal resistance. The interfacial conditions are thus written as:

$$q_1(L_1,t)=q_2(L_1,t) \tag{6}$$

$$q_1(L_1,t)=\tilde{\kappa}\left[T_1^4(L_1,t)-T_2^4(L_1,t)\right] \tag{7}$$

where $\tilde{\kappa}$ is a constant parameter dependent on the material properties of the films in contact [8,17]. Using the dimensionless variables:

$$\eta=\frac{t}{\tilde{\tau}_{qr}},\quad \zeta=\frac{x}{\sqrt{\alpha_r\tilde{\tau}_{qr}}},\quad \theta=\frac{T-T_r}{T_r},$$
$$Q=\frac{q}{c_rT_r\sqrt{\alpha_r/\tilde{\tau}_{qr}}},\quad \alpha_j=\frac{\tilde{\alpha}_j}{\alpha_r},\quad k_j=\frac{\tilde{k}_j}{k_r},\quad \tau_{qj}=\frac{\tilde{\tau}_{qj}}{\tilde{\tau}_{qr}},\quad \tau_{Tj}=\frac{\tilde{\tau}_{Tj}}{\tilde{\tau}_{qr}} \tag{8}$$

equations (1)–(7) are re-written in dimensionless form as:

$$\frac{\partial\theta_j}{\partial\eta}+\frac{\alpha_j}{k_j}\frac{\partial Q_j}{\partial\zeta}=0 \tag{9}$$

$$Q_j+\tau_{qj}\frac{\partial Q_j}{\partial\eta}+k_j\frac{\partial\theta_j}{\partial\zeta}+\tau_{Tj}k_j\frac{\partial^2\theta_j}{\partial\eta\partial\zeta}=0 \tag{10}$$

$$Q_1(\zeta,0)=0 \tag{11}$$

$$Q_2(\ell_1+\ell_2,\eta)=F(\eta) \tag{12}$$

$$\theta_j(\zeta,0)=\theta_j^o,\quad j=1,2 \tag{13}$$

$$Q_1(\ell_1,\eta)=Q_2(\ell_1,\eta) \tag{14}$$

$$Q_1(\ell_1,\eta)=\kappa\left[(\theta_1(\ell_1,\eta)+1)^4-(\theta_2(\ell_1,\eta)+1)^4\right] \tag{15}$$

where,

$$\kappa=\frac{\tilde{\kappa}T_r^3}{c_r\sqrt{\tilde{\tau}_{qr}/\alpha_r}},\quad \ell_j=\frac{L_j}{\sqrt{\alpha_r\tilde{\tau}_{qr}}} \tag{16}$$

3. Numerical solution method

Differentiating Eq. (9) with respect to ζ and substituting the result in Eq. (10) results in the following equation:

$$\tau_{Tj}\alpha_j\frac{\partial^2 Q_j}{\partial\zeta^2}-Q_j=\tau_{qj}\frac{\partial Q_j}{\partial\eta}+k_j\frac{\partial\theta_j}{\partial\zeta} \tag{17}$$

The descritization of Eq. (17) gives a tri-diagonal system of equations that can be efficiently solved using a tri-diagonal system solver as shown below. Using Crank–Nicolson Scheme, the descritization of Eqs. (17) and (9) gives:

$$A_i Q_{j,i-1}^{n+1} - B_i Q_{j,i}^{n+1} + C_i Q_{j,i+1}^{n+1} = -A_i Q_{j,i-1}^{n} + E_i Q_{j,i}^{n} - C_i Q_{j,i+1}^{n} + S_1\left(\delta\theta_{j,i}^{n} + \delta\theta_{j,i}^{p}\right) \tag{18}$$

$$\theta_{j,i}^{n+1} = \theta_{j,i}^{n} - S_2\left(\delta Q_{j,i}^{n} + \delta Q_{j,i}^{n+1}\right) \tag{19}$$

$$A_i = \frac{\tau_{Tj}\alpha_j \Delta\eta}{\Delta\zeta^2}, \quad B_i = \frac{2\tau_{Tj}\alpha_j \Delta\eta}{\Delta\zeta^2} + \Delta\eta + 2\tau_{qj},$$
$$C_i = \frac{\tau_{Tj}\alpha_j \Delta\eta}{\Delta\zeta^2}, \quad E_i = B_i - 4\tau_{qj} \tag{20}$$

$$S_1 = \frac{k_j \Delta\eta}{2\Delta\zeta}, \quad S_2 = \frac{\alpha_j \Delta\eta}{4k_j \Delta\zeta} \tag{21}$$

$$\delta\phi_{j,i} = \left\{ \begin{array}{ll} -3\phi_{j,i} + 4\phi_{j,i+1} - \phi_{j,i+2}, & i = 1 \\ \phi_{j,i+1} - \phi_{j,i-1}, & 1 < i < \mathrm{MI} \\ 3\phi_{j,i} - 4\phi_{j,i-1} + \phi_{j,i-2}, & i = \mathrm{MI} \end{array} \right\}, \quad \text{for layer 1} \tag{22}$$

$$\delta\phi_{j,i} = \left\{ \begin{array}{ll} -3\phi_{j,i} + 4\phi_{j,i+1} - \phi_{j,i+2}, & i = \mathrm{MI} \\ \phi_{j,i+1} - \phi_{j,i-1}, & \mathrm{MI} < i < M \\ 3\phi_{j,i} - 4\phi_{j,i-1} + \phi_{j,i-2}, & i = M \end{array} \right\}, \quad \text{for layer 2} \tag{23}$$

where $\delta\phi_{j,i}$ stands for $\delta\theta_{j,i}^{p}, \theta_{j,i}^{n}, \theta_{j,i}^{n+1}$, and MI is the grid point at the interface. The above equations are solved iteratively. Starting from an initial guess for $\theta_{j,i}^{p}$ with $\phi_{j,i}^{n}$ known from a previous time step, the tri-diagonal system of equations (18) is solved for the heat flux at the current time level, $Q_{j,i}^{n+1}$. Equation (19) is then solved for the temperature distribution, $\theta_{j,i}^{n+1}$ and is compared with the initial guess. If $|\theta_{j,i}^{n+1} - \theta_{j,i}^{p}| < \varepsilon$, convergence is achieved and the solution is advanced to the next time level, otherwise, the procedure is repeated after setting $\theta_{j,i}^{p} = \theta_{j,i}^{n+1}$ until convergence is achieved for all grid points. Once convergence is achieved, the temperature-dependent thermal boundary resistance $R_b(\kappa, \theta_1, \theta_2)$ is calculated by noting that Eq. (15) can be re-written as $R_b(\kappa, \theta_1, \theta_2) = [\theta_1(\ell_1, \eta) - \theta_2(\ell_1, \eta)]/Q_1(\ell_1, \eta)$.

4. Verification of the numerical procedure

The numerical scheme in the previous section is used to develop a Computer code for the analysis of transient energy transport in the two-layer film shown in Fig. 1. To check the accuracy of the numerical scheme and verify the results, the governing equations are solved using a semi-analytical method as explained below. The interfacial condition (Eq. (15)) can be re-written as:

$$Q_1(\ell_1, \eta) = \kappa[\theta_1 + \theta_2 + 2]\left[(\theta_1 + 1)^2 + (\theta_2 + 1)^2\right][\theta_1 - \theta_2] \tag{24}$$

or,

$$Q_1(\ell_1, \eta) = \frac{\theta_1 - \theta_2}{R_b(\kappa, \theta_1, \theta_2)} \tag{25}$$

where $R_b(\kappa, \theta_1, \theta_2)$ is the nonlinear temperature-dependent thermal boundary resistance given as:

$$R_b(\kappa, \theta_1, \theta_2) = \frac{1}{\kappa[\theta_1 + \theta_2 + 2]\left[(\theta_1 + 1)^2 + (\theta_2 + 1)^2\right]} \tag{26}$$

The interface approaches the perfect conditions with $\theta_1(\ell_1, \eta) = \theta_2(\ell_1, \eta)$ and $Q_1(\ell_1, \eta) = Q_2(\ell_1, \eta)$ as $\kappa \to \infty$ (i.e., $R_b(\kappa, \theta_1, \theta_2) \to 0$). Hence, a semi-analytical solution can be obtained using the Laplace transform method with a perfect contact interface ($R_b(\kappa, \theta_1, \theta_2) = 0$) as well as treating the interface as a perfect insulator ($R_b(\kappa, \theta_1, \theta_2) = \infty$) and the numerical scheme in the previous section can be assessed using these two limiting cases. These two limiting conditions however eliminate completely the nonlinear interfacial condition. Another approach of verification of the numerical scheme is to solve the governing equations using the Laplace transform method with the linearized form of the interfacial condition (Eq. (25)). However, the solution obtained is valid only for either very low (though non-zero) values of the thermal resistance R_b (i.e., very high values of the parameter κ) or infinitely high values of R_b. In this work and since the results all pertain to finite values of κ, the later path is taken even though it involves much algebraic manipulations and computational time. Taking the Laplace transform of Eqs. (9) and (10), and applying the initial conditions, $\theta_j(\zeta, 0) = 0$, $Q_j(\zeta, 0)$, $j = 1, 2$, one obtains after some manipulations the following equation for layer j:

$$\frac{\mathrm{d}^2\overline{\theta}_j}{\mathrm{d}\zeta^2} - A_j^2\overline{\theta}_j = 0 \tag{27}$$

where,

$$A_j = \sqrt{\frac{p(1 + \tau_{qj}p)}{\alpha_j(1 + \tau_{Tj}p)}} \tag{28}$$

and p is the Laplace transform parameter given by:

$$\overline{\theta}_j(\zeta, p) = \int_0^\infty \theta_j(\zeta, \eta)\mathrm{e}^{-p\eta}\mathrm{d}\eta \tag{29}$$

The solution to Eq. (27) is:

$$\overline{\theta}_j(\zeta, p) = D_{1j}\mathrm{e}^{A_j\zeta} + D_{2j}\mathrm{e}^{-A_j\zeta} \tag{30}$$

and the heat flux is given by:

$$\overline{Q}_j(\zeta, p) = -\frac{pk_j}{\alpha_j A_j}\left(D_{1j}\mathrm{e}^{A_j\zeta} - D_{2j}\mathrm{e}^{-A_j\zeta}\right) \tag{31}$$

The constants D_{1j}, D_{2j} are found by applying the boundary conditions as given by Eqs. (11), (12), (14) and (25) in the Laplace transform domain. This results in the following equations:

$$D_{21} = D_{11} \tag{32}$$

$$a_1 D_{11} - D_{12} - a_2 D_{22} = 0 \tag{33}$$

$$a_3 D_{11} - a_4 D_{12} + a_5 D_{22} = 0 \tag{34}$$

$$D_{12} - a_6 D_{22} = a_0\overline{F}(p) \tag{35}$$

The simultaneous solution to Eqs. (33)–(35) gives:

$$D_{11} = \frac{(a_5 + a_2 a_4)a_0\overline{F}}{a_1(a_5 - a_4 a_6) + a_3(a_2 + a_6)} \tag{36}$$

$$D_{12} = \frac{(a_2 a_3 + a_1 a_5)a_0\overline{F}}{a_1(a_5 - a_4 a_6) + a_3(a_2 + a_6)} \tag{37}$$

$$D_{22} = \frac{(a_1 a_4 - a_3)a_0\overline{F}}{a_1(a_5 - a_4 a_6) + a_3(a_2 + a_6)} \tag{38}$$

where,

$$a_0 = -\frac{\alpha_2 A_2 e^{-A_2(\ell_1+\ell_2)}}{k_2 p}, \quad a_1 = \left(1+\frac{R_b k_1 p}{\alpha_1 A_1}\right)e^{(A_1-A_2)\ell_1} + \left(1-\frac{R_b k_1 p}{\alpha_1 A_1}\right)e^{-(A_1+A_2)\ell_1} \tag{39}$$

$$a_2 = e^{-2A_2\ell_1}, \quad a_3 = \frac{k_1}{\alpha_1 A_1}\left(1-e^{-2A_1\ell_1}\right), \quad a_4 = \frac{k_2}{\alpha_2 A_2}e^{(A_2-A_1)\ell_1} \tag{40}$$

$$a_5 = \frac{k_2}{\alpha_2 A_2}e^{-(A_1+A_2)\ell_1}, \quad a_6 = e^{-2A_2(\ell_1+\ell_2)} \tag{41}$$

The Laplace inversion of the above equations is computed using the Riemann sum approximation given by [9]:

$$\Phi(\zeta,\eta) \cong \frac{e^{\gamma\eta}}{\eta}\left[\frac{1}{2}\overline{\Phi}(\zeta,\gamma) + \mathrm{Re}\sum_{n=1}^{N}\overline{\Phi}\left(\zeta,\gamma+\frac{in\pi}{\eta}\right)(-1)^n\right] \tag{42}$$

where $\Phi, \overline{\Phi}$ stands for $\theta, \overline{\theta}$ or $Q, \overline{Q}$ respectively, $i = \sqrt{-1}$ and $\gamma\eta \cong 4.7$ gives the most satisfactory results in terms of convergence rate [9] of the Riemann sum. The Riemann sum approximation technique is a common and reliable method and as stated in [9] it has been rigorously examined and proved to give satisfactory results in terms of convergence. A computer code is developed to solve the above equations for the temperature and heat flux distributions. Since the thermal boundary resistance (Eq. (26)) is a function of temperature, an iteration procedure is required. This is summarized below:

1. Assume a value for R_b.
2. Calculate the temperature distribution.
3. Calculate R_b from Eq. (26) using the temperatures calculated in step (2).
4. If the absolute difference between the assumed and calculate values of R_b falls below a specified tolerance, convergence is achieved, otherwise step (2) is repeated with the calculated value of R_b and the procedure is continued until convergence is achieved.

The grid size and the convergence criterion are taken as $\Delta\zeta = 0.002$, $\varepsilon = 10^{-10}$ for both solution methods and the time step is taken as $\Delta\eta = 5\times10^{-6}$. In this work, the thermal diffusivities of the two layers are taken as $\alpha_1 = \alpha_2 = 1.0$, while the thermal conductivity of layer 1 is taken as $k_1 = 1.0$, and the widths of the two layers are taken as $\ell_1 = \ell_2 = 0.5$. The initial temperatures of the two layers are set as $\theta_1(\zeta,0) = \theta_2(\zeta,0) = 0$ and the phase lags of the heat flux are taken as $\tau_{q1} = \tau_{q2} = 1.0$ unless otherwise stated on the relevant plots. The temperature gradient phase lags are taken as $\tau_{T1} = \tau_{T2} = 0.01$ forcing the DPL model to be more hyperbolic with thermal wave nature of energy transport. This choice of phase lags ($\tau_T << \tau_q$) imposes the most stringent resolution requirement in this study, and a satisfactory solution with this choice is necessarily adequate for any choice with $\tau_q = 1.0$ and $\tau_T > 0.01$.

The time dependent thermal pulse on the outer surface of layer 2 is taken in this study as a sinusoidal pulse of the form:

$$f(t) = \begin{cases} -q_s \sin(\pi t/t_s), & 0 \le t \le t_s \\ 0, & t > t_s \end{cases} \tag{43}$$

where q_s is the strength of the thermal pulse, and t_s is the pulse duration. The minus sign indicates that the heat pulse is in the negative ζ-direction. A sinusoidal thermal pulse is used in this study though any other shape of the pulse could be used that can be in turn represented by a Sine or Cosine Fourier series. The use of the sinusoidal thermal pulse (Eq. (43)) can resemble a laser pulse that is widely used in engineering applications. The dimensionless form of $f(t)$ is:

$$F(\eta) = \begin{cases} -Q_s \sin(\pi\eta/\eta_s), & 0 \le \eta \le \eta_s \\ 0, & \eta > \eta_s \end{cases} \tag{44}$$

The thermal pulse duration and intensity are taken as $\eta_s = 0.2$, $Q_s = 1.0$ throughout the whole study.

A comparison between the finite difference numerical solution and the semi-analytical Laplace transform-based solution is made in Fig. 2, where both the temperature and heat flux distributions in the two-layer structure are shown at time $\eta = 0.8$. At this time, the thermal pulse has already interacted with the interface. With the values chosen for the phase lags of the heat flux and temperature gradient, the wave nature of energy transport is dominant and it takes around $\eta = 0.5$ for the thermal pulse generated at the right boundary of layer 2 to reach the interface. Fig. 3 shows the variation with time of the temperature difference and heat flux at the interface together with the thermal resistance, corresponding to those shown in Fig. 2. The duration taken in Fig. 3 is $\eta = 2.0$, where the thermal pulse has propagated through the two layers, reflected back from the left surface of layer 1 and reached the outer surface of layer 2. The thermal boundary resistance corresponding to $\kappa = 1.0$ at the initial temperatures $\theta_1(\zeta,0) = \theta_2(\zeta,0) = 0$ calculated from Eq. (26) is $R_b = 0.25$. Since a value of $\kappa = 1.0$ results in a relatively large interfacial resistance, a considerable difference between the two solutions is observed, though both solutions qualitatively capture the thermal pulse transmission and reflection from the interface. This is because the Laplace transform solution method with the linearization of the interfacial condition is only accurate when $R_b(\kappa,\theta_1,\theta_2)\to 0$ where the interface approaches the perfect conditions. To ensure that the large difference between the two solutions is due to the linearization of the nonlinear interfacial condition R_b not the numerical method, the previous computations are repeated in Figs. 4 and 5 but with $\kappa = 50.0$. The thermal boundary resistance corresponding to $\kappa = 50.0$ at the initial temperatures $\theta_1(\zeta,0) = \theta_2(\zeta,0) = 0$ is calculated from Eq. (26) as $R_b = 0.005$, and since $R_b \sim \theta_I^{-3}$, this value is the highest during the process of energy transport. For this low value of thermal resistance, the interface approaches the perfect conditions with almost zero temperature difference at the interface. The difference

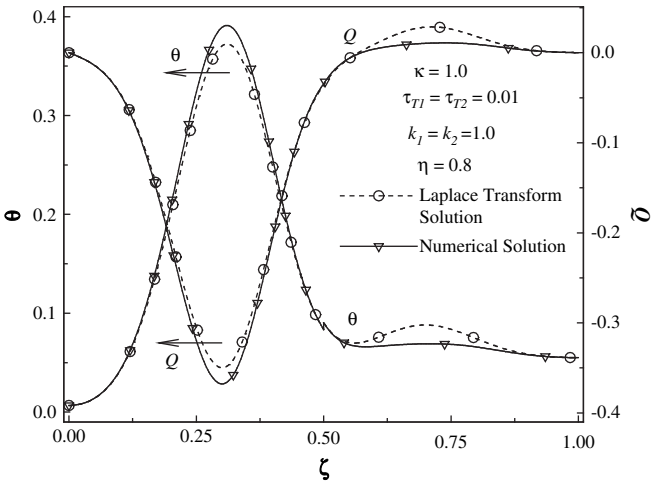

Fig. 2. Temperature and heat flux distributions at $\eta = 0.8$: A comparison between numerical and Laplace transform solution methods for a high interfacial resistance.

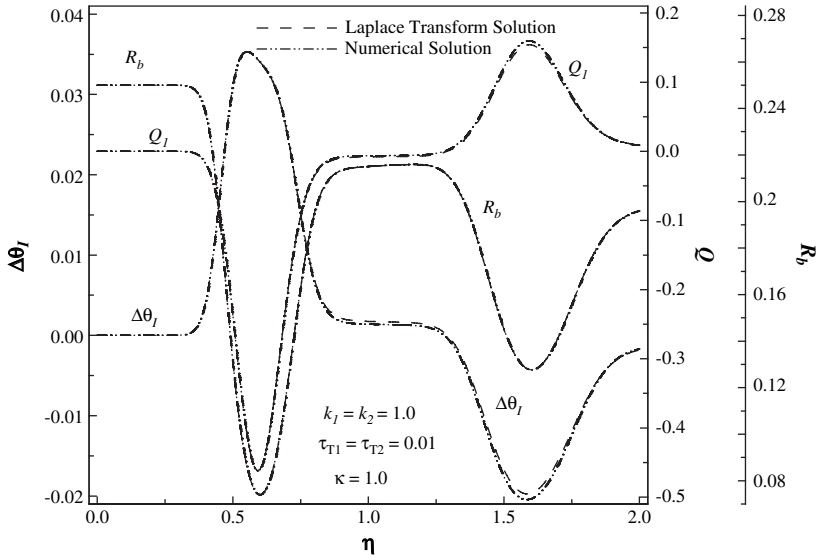

Fig. 3. Variation of the thermal boundary resistance, temperature difference and heat flux at the interface for $\kappa = 1.0$: A comparison between the numerical and the Laplace transform solution methods.

between the two solutions is unnoticeable as is clear from Figs. 4 and 5. The numerical solution method is thus capable of resolving the thermal wave propagation in the two layers and thermal wave transmission and reflection at the interface quite accurately.

5. Results and discussion

Before proceeding in the analysis of the effects of the thermophysical properties of the two layers on energy transport through the interface, it is noticed from Figs. 4 and 5 that for a low-thermal boundary resistance, the interface transmits most of the thermal pulse with a negligible interfacial temperature difference. The temperature dependent thermal boundary resistance is the highest at the initial temperatures (Fig. 5). The interfacial temperature difference $\Delta\theta_1$ remains almost zero until around $\eta \approx 0.4$ where the thermal pulse has not yet reached the interface. Hence, the thermal boundary resistance remains almost constant during this period. The first sharp change of $\Delta\theta_1$ in the range $\eta \approx 0.4$ and $\eta \approx 0.8$ is due

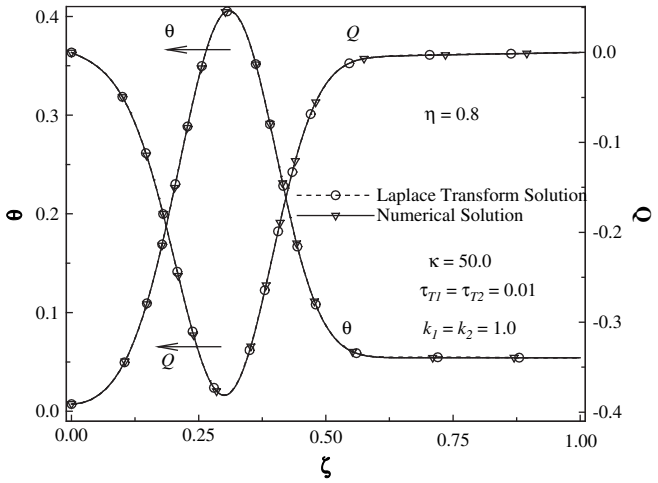

Fig. 4. Temperature and heat flux distributions at $\eta = 0.8$: A comparison between numerical and Laplace transform solution methods for a low interfacial resistance.

the fact that the thermal wave has started passing through the interface towards the left surface of layer 1. This is accompanied by a sharp change in the thermal resistance as both θ_1, θ_2 become higher than their respective initial values. The second sharp change in $\Delta\theta_1$ and consequently in R_b starts at around $\eta \approx 1.3$ where the reflected thermal wave from the left surface of layer 1 has reached the interface.

In the following analysis, the effects on energy transport of the temperature-dependent thermal boundary resistance, thermal conductivities, and phase lags of the two layers are investigated. Fig. 6 shows the temperature distribution at $\eta = 0.8$ in the two-layer slab with similar materials for different values of the parameter κ. Thermal wave reflections and transmissions at the interface are clearly shown, where the thermal wave reflected from the interface propagates to the right, while the wave transmitted through the interface propagates towards the left surface of layer 1. For $\kappa = 0.001$ (high-thermal resistance), the interfacial temperature difference is the highest, where most of the thermal pulse is reflected from the interface towards the outer surface of layer 2 with only little energy transmitted through the interface. The value of $\kappa = 1.0$ (low-thermal resistance) conversely results in the lowest interfacial temperature difference, where most of the thermal pulse is transmitted through the interface. The value of the parameter κ and hence the thermal boundary resistance has a considerable effect on energy transport and temperature variations in the two layers.

To see the effect of the thermal conductivities and heat capacities of the two layers on energy transport in the two-layer slab, a snapshot (at $\eta = 0.8$) of the temperature distribution is shown in Fig. 7 for different values of the thermal conductivity of layer 2 and with a high value of thermal resistance ($\kappa = 0.001$). With the parameters chosen, the thermal conductivity and heat capacity ratios of the two layers are equal, (i.e., $k_2/k_1 = c_2/c_1$). The graph corresponding to $k_2 = 0.1$ in Fig. 7 shows the highest interfacial temperature difference with a considerable portion of the thermal pulse crossing the interface and propagating towards the outer surface of layer1 even with a high value of the interfacial resistance. The interface also reflects a positive wave followed by a negative wave both propagating towards the outer surface of layer 2 where the temperature in some portions of layer 2 drops below the initial

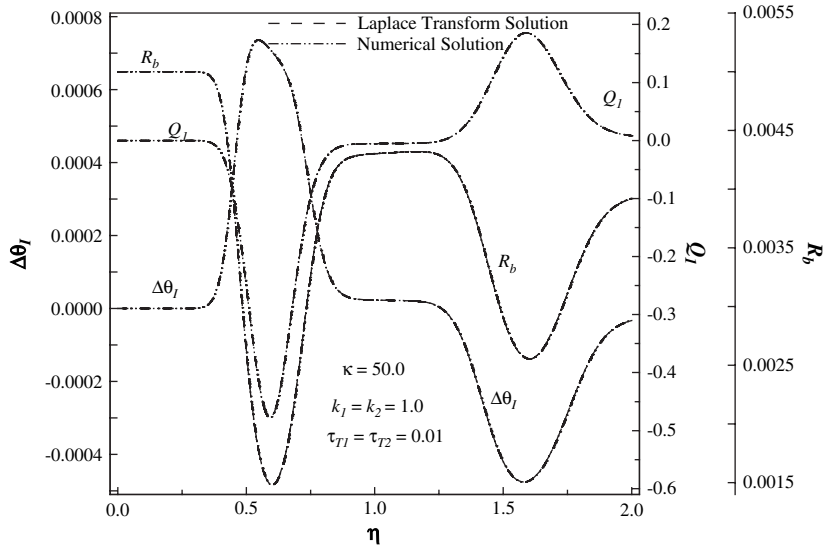

Fig. 5. Variation of the thermal boundary resistance, temperature difference and heat flux at the interface for $\kappa = 50.0$: A comparison between the numerical- and the Laplace transform solution methods.

temperature. The graph corresponding to $k_2 = 100.0$ on the other hand shows a vanishing interfacial temperature difference even though the thermal resistance is high. The transmitted and reflected thermal waves are also of vanishing strengths. Fig. 7 also shows that as the value of k_2 (and hence c_2/c_1) increases, both the transmitted and reflected waves become weaker with a decreasing role of the interfacial resistance. This shows that when a thermal pulse propagates from a layer of high-thermal conductivity and heat capacity to a low-thermal conductivity and heat capacity layer, the interface approaches the perfect contact conditions even with high values of thermal boundary resistance. On the other hand, propagation of a thermal pulse from a low conductivity and heat capacity towards a high conductivity and heat capacity layer results in higher interfacial temperature difference. This is due to the fact that with increasing the heat capacity and thermal conductivity, layer 2 behaves more as a heat sink with increasing capability to absorb the energy transmitted via the boundary heat flux. This results in decreasing the amplitude of the thermal pulse propagating towards the interface (less temperature rise in layer 2) and hence less interfacial temperature difference. A more clear representation of the effect of the thermal conductivities and heat capacities on the temperature difference and heat flux at the interface is shown in Fig. 8 where the variation with time of the interfacial quantities is shown during the propagation of the thermal pulse from layer 2 towards layer 1. The time duration is taken as $\eta = 1.0$ to ensure that the thermal pulse initiated at $\eta = 0.0$ at the right surface of layer 2 has reached the left surface of layer 1 for any choice of the temperature gradient and heat flux phase lags. As the thermal conductivity of layer 2 is increased, both the interfacial temperature difference and the heat flux crossing the interface decrease (Q is negative since the thermal pulse propagates in the negative ζ direction). The peak values of the interfacial quantities occur at around $\eta \approx 0.6$ where the thermal pulse (of duration $\eta_s = 0.2$) has completely interacted with the interface.

Fig. 8 however represents a case with the two layers having the same values of τ_T and τ_q. Next, the effect of the temperature

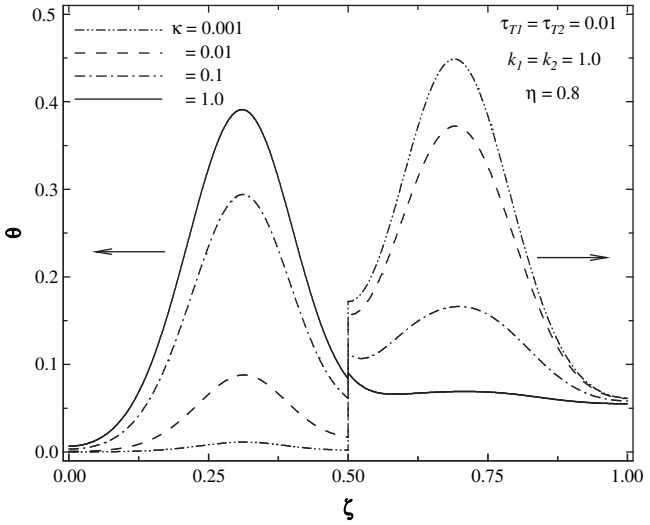

Fig. 6. Temperature distribution at $\eta = 0.8$ in a two-layer film of the same material for different values of the interfacial resistance.

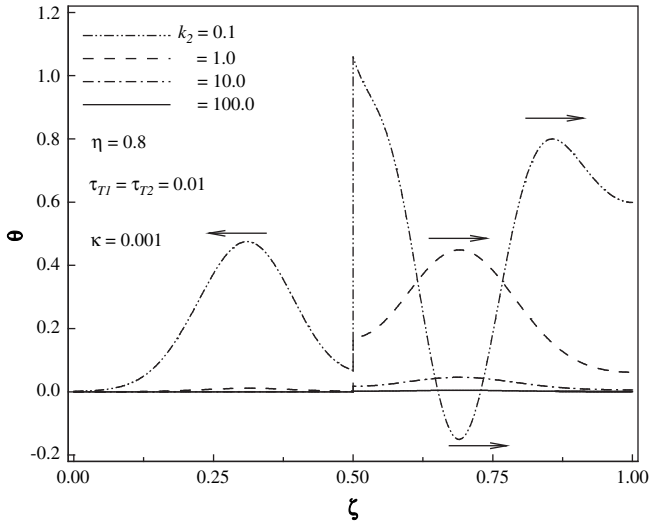

Fig. 7. Temperature distribution at $\eta = 0.8$ in two-layer film for different values of the thermal conductivity of layer 2.

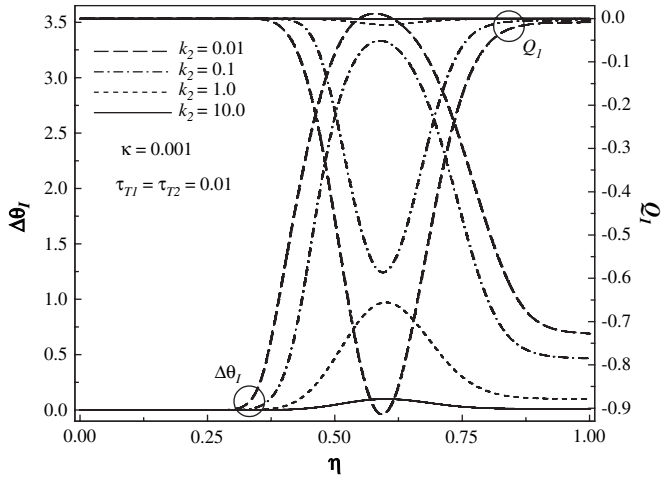

Fig. 8. Effect of the thermal conductivity of layer 2 on the temporal interfacial temperature difference and heat flux for $\tau_{T1} = \tau_{T2} = 0.01$.

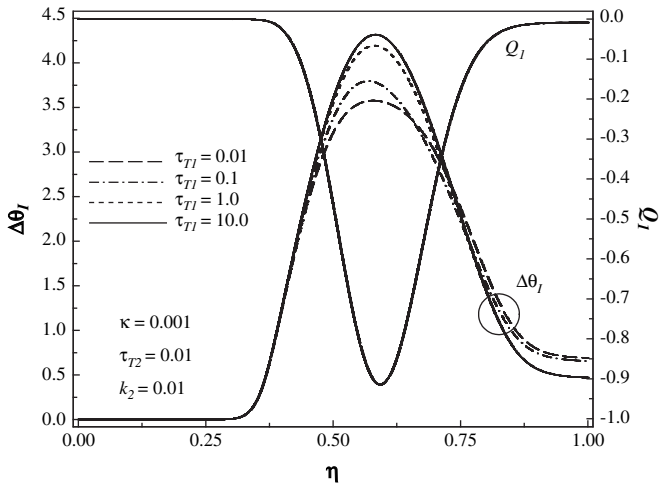

Fig. 10. Temporal variation of the temperature difference and heat flux at the interface with $\kappa = 0.001, k_2 = 0.01$ and $\tau_{T2} \le \tau_{T1}$.

gradient and heat flux phase lags on heat transfer at the imperfect interface is investigated. The temporal variation of the interfacial quantities $\Delta\theta_I$ and Q_I is represented in Fig. 9 for a thermal pulse propagating from a low τ_T layer ($\tau_{T2} = 0.01$) to a higher τ_T layer ($\tau_{T1} = 0.1$). The thermal conductivities and thermal resistance are the same as in Fig. 8. Comparing Figs. 8 and 9, the phase lags clearly have some effect on the interfacial quantities with higher values of these quantities when the thermal pulse propagates from a lower-to-higher τ_T layer. The effect of the phase lags on the temporal variation of $\Delta\theta_I$ and Q_I is further studied as shown in Figs. 10–13, where the thermal pulse propagates through layer 2 towards layer 1 with $\tau_{T2} \le \tau_{T1}$ in Fig. 10 and $\tau_{T2} \ge \tau_{T1}$ in Fig. 11, while in Figs. 12 and 13 the thermal pulse propagates through layer 2 towards layer 1 with $\tau_{q2} \ge \tau_{q1}$ and $\tau_{q2} \le \tau_{q1}$ respectively. The values of k_2 and κ are the same in these four figures. With the parameters chosen, the heat flux at the interface is the same for the four cases shown in these figures where the four curves of Q_I corresponding to the four cases coincide, while the interface shows a variable response in terms of the interfacial temperature difference. In other words, the same heat flux crossing the interface results in different values of the interfacial temperature difference depending on the phase lags of the two layers. The results presented in Figs. 8–13 thus clearly show that within the framework of the DPL model the interfacial temperature difference $\Delta\theta_I$ is the proper choice to measure the perfect-ness of the interface rather than the interfacial heat flux Q_I. It can be also noticed from these figures that the peak values of $\Delta\theta_I$ and Q_I take place at different times. This may be explained by the fact that within the DPL model, the heat flux lags behind the temperature gradient when $\tau_q > \tau_T$, and the temperature gradient lags behind the heat flux when $\tau_T > \tau_q$, while the heat flux and temperature gradient are simultaneous when $\tau_T = \tau_q$. The response of the interface to the thermal pulse is instantaneous when the thermal pulse propagates from layer 2 towards layer 1 with $\tau_{T2} \ge \tau_{T1}$ (Fig. 11), where the nature of energy transport is enhanced diffusion with $\tau_{T2} > \tau_{q2}$. The interfacial quantities $\Delta\theta_I$ and Q_I reach their peak values at around $\eta \sim 0.12$ even before the termination of the thermal pulse. On the other hand, with $\tau_{T2} \le \tau_{T1}$ (Fig. 10), thermal wave nature dominates the energy transport process ($\tau_{T2} < \tau_{q2}$), where it takes around $\eta \approx 0.35$ for the thermal pulse to interact with the interface, and the interfacial quantities peak at around $\eta \sim 0.6$.

The conclusions that are drawn from the previous analysis is that in addition to the thermal boundary resistance, the thermal

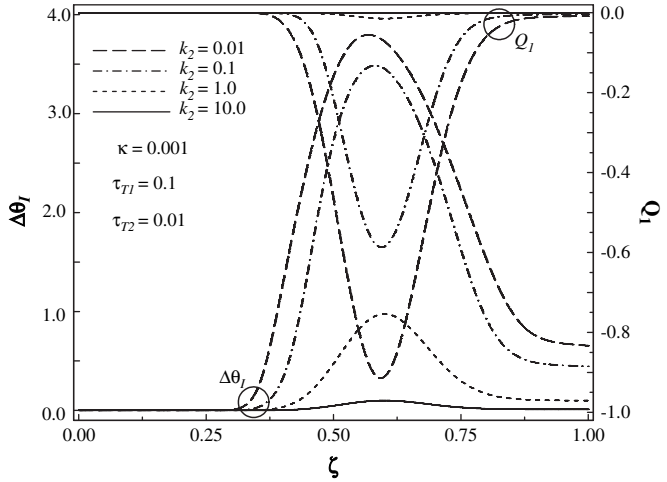

Fig. 9. Effect of the thermal conductivity of layer 2 on the temporal interfacial temperature difference and heat flux for $\tau_{T1} = 0.1$ and $\tau_{T2} = 0.01$.

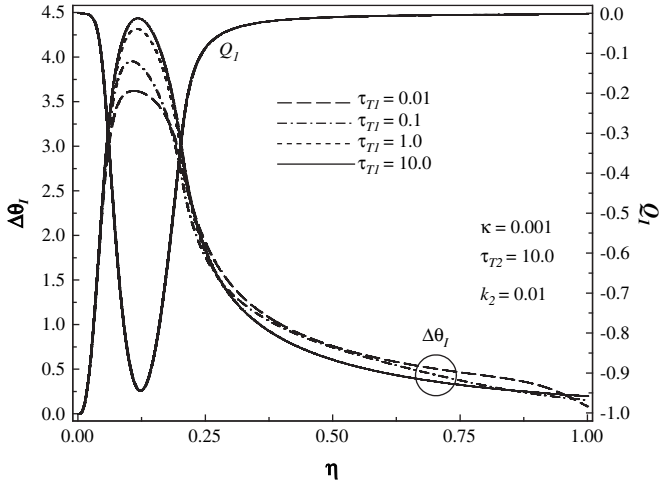

Fig. 11. Temporal variation of the temperature difference and heat flux at the interface for $\kappa = 0.001, k_2 = 0.01$ and $\tau_{T2} \ge \tau_{T1}$.

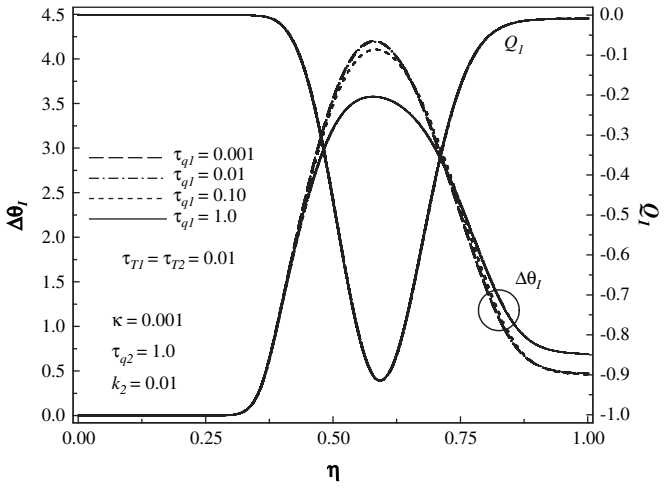

Fig. 12. Temporal variation of the temperature difference and heat flux at the interface for $\kappa = 0.001$, $k_2 = 0.01$ and $\tau_{q2} \geq \tau_{q1}$.

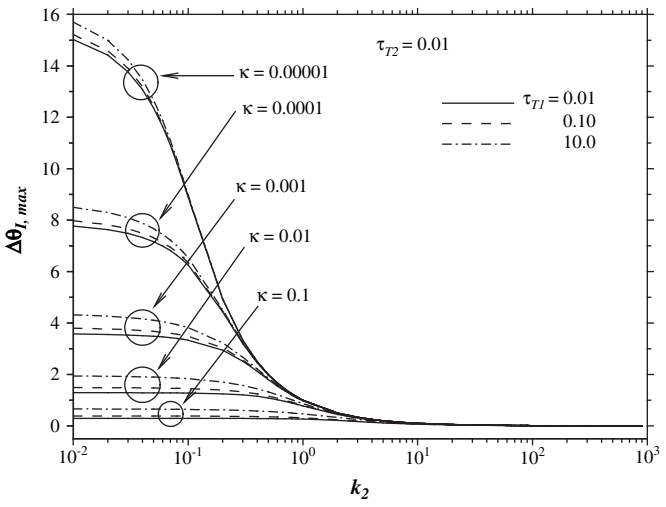

Fig. 14. Variation of the maximum interfacial temperature difference with the thermal conductivity of layer 2 for $\tau_{T2} \leq \tau_{T1}$ and a range of the parameter κ.

conductivities and the phase lags play important roles in determining the interfacial temperature difference and the heat flux passing through the interface. Propagation of a thermal pulse from a high-to-low thermal conductivity layers results in lower interfacial temperature difference and less energy crossing the interface. In addition, higher difference between the temperature gradient phase lags of the two layers, results in lower interfacial temperature difference (Figs. 10 and 11), whereas for $\tau_{q2} \geq \tau_{q1}$ (Fig. 12), higher difference between the heat flux phase lags results in higher maximum interfacial temperature difference, while for $\tau_{q2} \leq \tau_{q1}$, higher difference between the heat flux phase lags results in lower maximum interfacial temperature difference. Moreover, Figs. 10–13 show that the effect of the phase lags of the heat flux and temperature gradient are comparable. The interface is perfect when the thermal boundary resistance $R_b \to 0$ or $\kappa \to \infty$, where in this case $\Delta\theta_I \to 0$ and $Q_1 = Q_2$ at the interface. The previous results particularly those shown in Figs. 8 and 9 show that $\Delta\theta_I$ approaches zero even with a relatively high-thermal boundary resistance (low κ). Due to this fact in addition to the results shown in Figs. 10–13, the interfacial temperature difference is considered to be the proper choice to measure the relative perfect-ness of the interface.

Figs. 8–13 show that the interfacial temperature difference takes on a unique maximum value during the passage of the thermal pulse through the interface. Thus the maximum value of the interfacial temperature difference that takes place during the thermal pulse propagation from layer 2 towards layer 1 is taken as a measure of the relative perfect-ness of the interface. Extensive computations are performed to locate the maximum interfacial temperature difference $\Delta\theta_{I,\max}$ for different values of $\kappa, k_2, \tau_{T1}, \tau_{T2}$ and the results are presented in Figs. 14–16. Figs. 14 and 15 indicate that the values of the phase lags have much less effect on $\Delta\theta_{I,\max}$ than those of κ and k_2. As k_2 increases $\Delta\theta_{I,\max}$ decreases with a decreasing effect of the thermal resistance (κ), so that when $k_2 \geq 10$, $\Delta\theta_{I,\max} \to 0$ where the value of κ becomes insignificant and the behavior of the interface approaches that of a perfect interface regardless of the value of the interfacial resistance. As k_2 decreases $\Delta\theta_{I,\max}$ increases where the increase in $\Delta\theta_{I,\max}$ is governed by the thermal resistance. Fig. 16 shows the variation of $\Delta\theta_{I,\max}$ with κ for different values of k_2. Clearly as κ increases (thermal resistance decreases) or k_2 increases the interface approaches the perfect conditions, and with $k_2 = 10$, $\Delta\theta_{I,\max} \to 0$ for the whole range of κ shown.

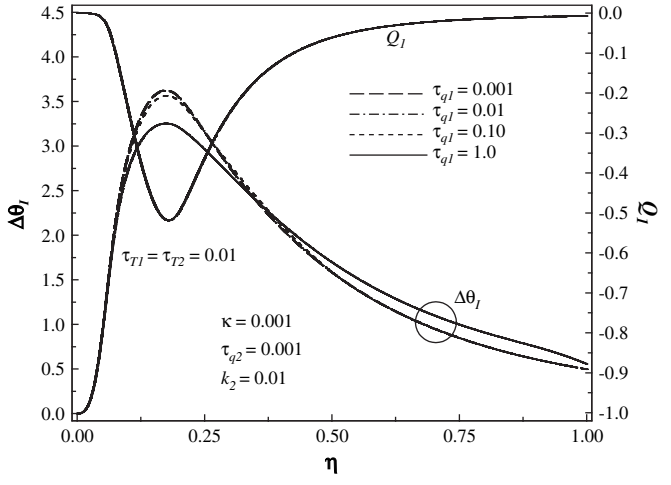

Fig. 13. Temporal variation of the temperature difference and heat flux at the interface for $\kappa = 0.001, k_2 = 0.01$ and $\tau_{q2} \leq \tau_{q1}$.

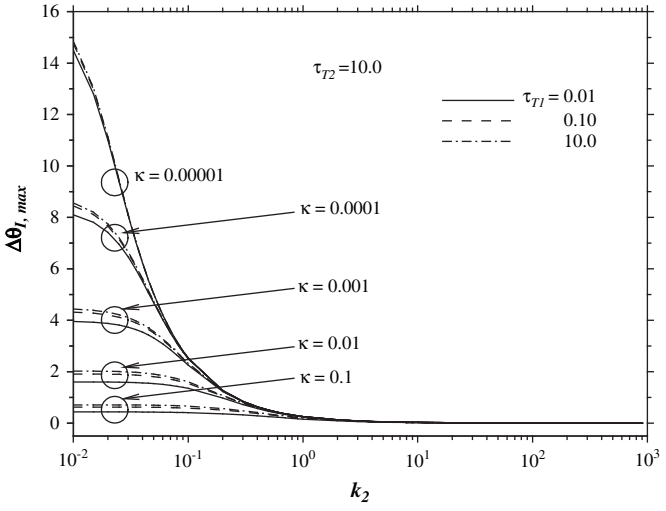

Fig. 15. Variation of the maximum interfacial temperature difference with the thermal conductivity of layer 2 for $\tau_{T2} \geq \tau_{T1}$ and a range of the parameter κ.

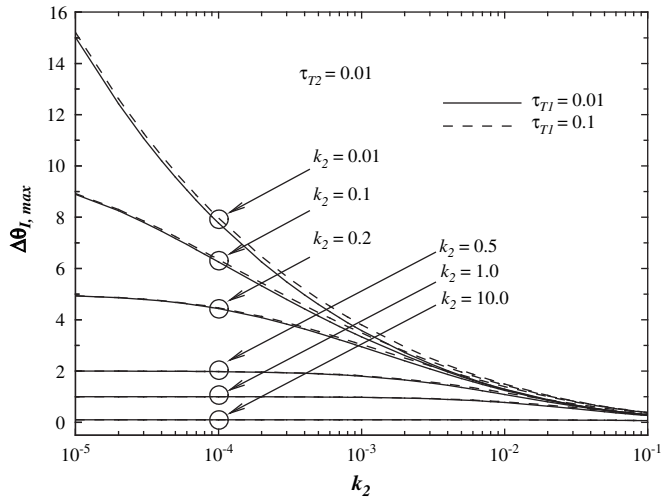

Fig. 16. Variation of the maximum interfacial temperature difference with the parameter κ for different values of the thermal conductivity of layer 2.

6. Conclusions

Analysis of energy transport in two-layer thin films with a nonlinear thermal boundary resistance is performed using an iterative finite difference numerical method that is second order accurate in both time and space. The numerical solution method is verified using a derived semi-analytical solution. The concentration in this work is on the effects of the thermo-physical properties on energy transport in a two-layer planar slab with a temperature dependent thermal boundary resistance when one layer is exposed to an external thermal pulse.

The interfacial thermal boundary resistance, the heat flux and temperature gradient phase lags and the thermal conductivities and heat capacities are all important factors that characterize and quantify energy transport through the interface and temperature distribution in the two layers. Since the dependency of the thermal boundary resistance on temperature is $R_b \sim \theta^{-3}$, it attains its highest value at the initial temperatures when heat is transferred to the composite geometry and it starts decreasing as the temperatures at the interface increase due to heat transfer. In the two extremes when $R_b \to 0$ and $R_b \to \infty$, the interfacial temperature difference respectively approaches zero with perfect contact conditions, and the largest possible difference where the interface behaves as a perfect insulator with vanishing heat flux crossing it. However, the interfacial temperature difference is considerably influenced by the thermo-physical properties of the layers as well as the nature of energy transport in the two layers. The results show that the thermal conductivities and heat capacities have much more effect on energy transport in the two-layer slab than those of the phase lags of the temperature gradient and heat flux. The maximum interfacial temperature difference $\Delta\theta_{I,\max}$ during thermal pulse propagation from one layer into another through the interface is chosen to measure the relative perfect-ness of the interface. The results show that even with high values of the thermal boundary resistance the maximum interfacial temperature difference can be very small when the thermal pulse propagates from a high-thermal conductivity and heat capacity layer to a low-thermal conductivity and heat capacity layer, and when $k_2/k_1 = C_2/C_1 \geq 10$, results show that the maximum interfacial temperature difference $\Delta\theta_{I,\max} \to 0$. On the other hand, propagation of a thermal pulse from a low-thermal conductivity and heat capacity layer to a high-thermal conductivity and heat capacity layer increases the interfacial temperature difference.

References

[1] S. Shaikh, K. Lafdi, E. Silerman, The effect of a CNT interface on the thermal resistance of contacting surfaces, Carbon 45 (2007) 695–703.
[2] M. Grujicic, C.L. Zhao, E.C. Dusel, The effect of thermal contact resistance on heat management in the electronic packaging, Appl. Surf. Sci. 246 (2005) 290–302.
[3] E.T. Swartz, R.O. Pohl, Thermal boundary resistance, Rev. Mod. Phys. 61 (1989) 605–668.
[4] R.S. Prasher, P.E. Phelan, A scattering-mediated acoustic mismatch model for the prediction of thermal boundary resistance, ASME J. Heat Transfer 123 (2001) 105–112.
[5] R.S. Prasher, Thermal boundary resistance of nanocomposites, Int. J. Heat Mass Transfer 48 (2005) 4942–4952.
[6] A. McDonald, C. Moreau, S. Chandra, Thermal contact resistance between plasma-sprayed particles and flat surfaces, Int. J. Heat Mass Transfer 50 (2007) 1737–1749.
[7] D.G. Cahill, Heat transport in dielectric thin films and at solid–solid interfaces, in: C.L. Tien, A. Majumdar, F.M. Gerner (Eds.), Microscale Energy Transport, Taylor and Francis, Washington, DC, 1998, pp. 95–117.
[8] W.B. Lor, H.S. Chu, Effect of interface thermal resistance on heat transfer in a composite medium using the thermal wave model, Int. J. Heat Mass Transfer 43 (2000) 653–663.
[9] D.Y. Tzou, Macro- to Microscale Heat Transfer: The Lagging Behavior, Taylor & Francis, Washington, DC, 1997.
[10] D.Y. Tzou, Experimental support for the lagging response in heat propagation, AIAA J. Thermophys. Heat Transfer 9 (1995) 686–693.
[11] J.R. Ho, C.P. Kuo, W.S. Jiaung, Study of heat transfer in multilayered structure within the framework of dual-phase-lag heat conduction model using lattice Boltzmann method, Int. J. Heat Mass Transfer 46 (2003) 55–69.
[12] N.S. Al-Huniti, M.A. Al-Nimr, Thermo elastic behavior of a composite slab under a rapid dual-phase-lag heating, J. Thermal Stresses 27 (2004) 607–623.
[13] Y.M. Lee, T.W. Tsai, Ultra-fast pulse-laser heating on a two-layered semi-infinite material with interfacial contact conductance, Int. Comm. Heat Mass Transfer 34 (2007) 45–51.
[14] M.A. Al-Nimr, M. Naji, R.I. Abdallah, Thermal behavior of a multi-layered thin slab carrying pulsating signals under the effect of the dual-phase-lag heat conduction model, Int. J. Thermophys. 25 (2004) 949–966.
[15] C.S. Tsai, C.I. Hung, Thermal wave propagation in a bi-layered composite sphere due to a sudden temperature change on the outer surface, Int. J. Heat Mass Transfer 46 (2003) 5137–5144.
[16] K.C. Liu, Analysis of dual-phase-lag thermal behavior in layered films with temperature-dependent interface thermal resistance, J. Phys. D: Appl. Phys. 38 (2005) 3722–3732.
[17] K.C. Liu, Analysis of thermal behavior in multi-layer metal thin films based on hyperbolic two-step model, Int. J. Heat Mass Transfer 50 (2007) 1397–1407.
[18] A.F. Khadrawi, M.A. Al-Nimr, M. Hammad, Thermal behavior of perfect and imperfect contact composite slab under the effect of the hyperbolic heat conduction model, Int. J. Thermophys. 23 (2002) 581–598.